DESIGN AND RESEARCH ON FEEDING COMPONENTS OF WHEAT FLOUR PARTICLE SIZE DETECTION DEVICE
/
小麦制粉粒度检测装置供料部件设计与研究

Mingxu WANG[1,2], Haojun ZHAO[1], Saiqiang LI[1], Jiangfeng OUYANG[1], Junyong WU[3], Hengda ZHANG[4]
School of Mechanical & Electrical Engineering, Henan University of Technology, Zhengzhou 450001, China
Henan Key Laboratory of Grain and Oil Storage Facility & Safety, Henan University of Technology, Zhengzhou 450001, China
Hebei Pingle Flour Machinery Group Co., Ltd., Zhengding 050800, China
Buler (Wuxi) Commercial Co., Ltd., Wuxi, Jiangsu 214142, China
Tel: 18623717728.; E-mail: wmx20032002@163.com
DOI: https://doi.org/10.35633/inmateh-73-03

Keywords: *Wheat milling; particle size detection; shaftless screw; Box-Behnken model*

ABSTRACT

To address the issues of poor timeliness and delayed feedback in traditional wheat milling processes for manual particle size detection, a wheat milling online particle size detection device has been designed. This paper focuses on the design optimization of the key feeding component in the device, which affects the accuracy of particle size detection. The feeding component adopts shaftless screw blades. Through theoretical analysis, the main parameter ranges affecting the throughput capacity of the shaftless screw conveyor are determined. A Box-Behnken experiment is designed to obtain the optimal parameter combination for each factor: outer diameter of screw blades 23.8 mm, inner diameter of screw blades 6.4 mm, pitch 11.2 mm, and blade rotation speed 288.9 r/min. Simulation and test stand experiments are conducted using the above parameter combination. The simulation results show that the average throughput capacity of the feeding component is 2.85 kg/h, while the average throughput capacity of the test stand experiment is 2.84 kg/h, with a coefficient of variation of uniformity of 1.33%. These results indicate that the above parameter combination meets the design requirements for the feeding component in the device.

摘要

针对传统小麦制粉工艺人工粒度检测时效性差、反馈迟滞等问题，设计了小麦制粉在线粒度检测装置，本文针对装置中的影响装置检测准确率的关键供料部件进行设计优化。供料部件采用无轴螺旋叶片，通过理论分析确定影响无轴螺旋输送能力的主要参数取值范围，设计 Box-Behnken 试验得到各因素的最优参数组合为：螺旋叶片外径 23.8mm，螺旋叶片内径 6.4mm，螺距 11.2mm，叶片转速 288.9r/min。采用上述参数组合进行仿真与台架试验，仿真结果为供料部件平均输送能力为 2.85kg/h，台架试验的平均输送能力为 2.84kg/h，均匀性变异系数为 1.33%，结果表明上述参数组合能够满足装置中供料部件的设计要求。

INTRODUCTION

In wheat milling, the particle size curve of the ground material serves as a direct indicator of the milling machine's technical efficiency (*Zhao et al, 2009*). Traditional flour mills typically rely on manual sieving to determine the particle size distribution of the ground material (*Wen et al, 2013*), leading to issues like poor timeliness, delayed feedback, and an inability to detect subtle fluctuations in processing quality. To address these challenges, the development of an online particle size detection equipment for the wheat milling industry is imperative. While online particle size detection technology has been extensively researched in industries like mining and coal mining (*Wang et al, 2018; Li et al, 2021; Wang et al, 2021; Bidas et al, 2021*), its application in wheat milling is still in its nascent stages. This paper proposes a novel approach based on the dynamic image method (*Yang., 2018*), introducing an online particle size detection device for wheat processing during the milling process. This device not only resolves the limitations of traditional manual offline detection methods but also facilitates seamless integration with milling machines, enabling automated and real-time adjustment of grinding parameters.

In terms of material feeding in the equipment, the application of shaftless screw blade mechanisms is ideal for the wheat milling industry, which demands strict cost and energy consumption control along with long equipment lifespans. Shaftless screw blades possess the desired characteristics (*Cheng et al, 2016*; *Ananth et al, 2023*) and have been widely utilized in various industries in recent years. For instance, Ma designed a simulated lunar soil active filling device based on shaftless screw blade design principles (*Ma et al, 2019*).

Wang applied shaftless screw blades to biomass screw continuous pyrolysis equipment feeders, addressing issues such as high mass, energy consumption, and susceptibility to mechanical interference associated with shafted screw feeders (*Wang et al, 2017*). Jiang optimized the structural parameters of sterilizers' shaftless screw heating conveyors using a particle swarm algorithm and verified the optimized parameters using COMSOL software (*Jiang et al, 2020*). Orefice conducted an analysis of the effect of screw shaft size on material conveying efficiency using discrete element analysis, finding that smaller screw shafts led to higher productivity and efficiency (*Orefice et al, 2017*). Bangura designed a spiral groove wheel manure spreading device, and experimental verification revealed improvements in both manure discharge quantity and uniformity (*Bangura et al, 2020*).

This paper is based on the principle of shaftless screw conveying to design the key shaftless screw feeding component in the wheat milling particle size detection device. The structural parameters of the screw in the feeding component are crucial, as their stability directly affects the accuracy of particle size identification in the final device operation. Therefore, based on the throughput demand of the device process, the various parameters of the shaftless screw blades are designed. Utilizing the discrete element method, a quadratic regression orthogonal Box-Behnken combined experiment is conducted to determine the optimal combination of parameters for the screw conveying blades. Subsequently, experimental verification is performed on the test stand. This study aims to provide a reference for the design of wheat milling sub-material particle size detection devices and the optimization of shaftless screw design.

MATERIAL AND METHODS

The Overall Structure of The Device

The structural working principle of the wheat processing particle size detection device is illustrated in Figure 1. The device primarily consists of feeding components, a vibrating feeder, a collection box, a capturing unit, and a cleaning unit. Its operation relies on a PLC control system, with parameters controlled via a touchscreen interface. The working process of the device is as follows: sample material is fed into the particle size detection device from beneath the grinding roller via a Sampling component, where it vertically descends through the material inlet; the feeding device transports the sample material to the vibrating feeder; the material descends from the end of the vibrating feeder in a "single-layer material waterfall" form; the capturing unit captures images of the descending particles using backlighting; and the images are then analysed for particle size information using proprietary algorithms upon transmission to a computer. In practical applications, one PLC control system can manage multiple particle size detection devices.

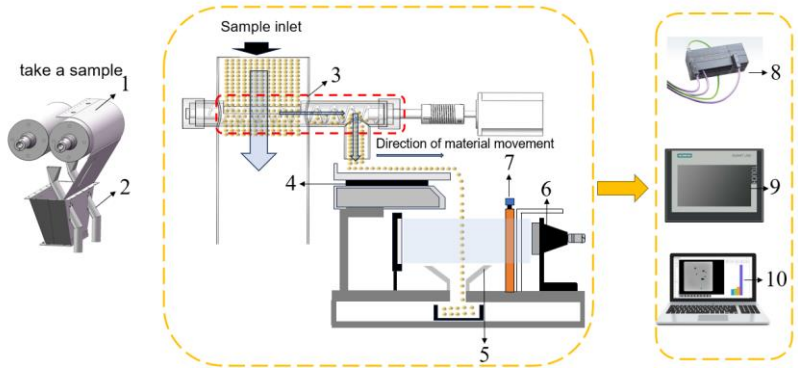

Fig. 1 - Device Structure and Working Principle

1- Grinding roller; 2-Sampling component; 3-Feeding component; 4-Vibrating feeder; 5-Collection box; 6-Capturing unit; 7-Cleaning unit; 8-PLC; 9-Touchscreens; 10-Recognition software

Feeding Component Working Principle

The material flows into the inlet pipe and falls into the entrance of the feeding component. The shaftless screw blade, driven by a stepper motor, continuously rotates in the specified direction. The material falls into the feeding trough of the vibrating feeder at the rear end of the feeding device.

Design of Shaftless Screw Blade Structure and Parameters

In order to ensure the conveying state and uniformity of materials when they are conveyed to the vibrating feeder, and to avoid blockages in the conveying device, it is crucial to maintain a stable conveying state of the materials. The conveying state of the materials ultimately affects the accuracy of particle size identification. When materials are in motion within the shaftless screw conveying device, the shape and size parameters of the shaftless screw directly influence the trajectory of the materials (*Motaln et al, 2017*).

Therefore, detailed design of the shaftless screw is required to determine key parameters such as the outer diameter, inner diameter, and pitch of the shaftless screw blades.

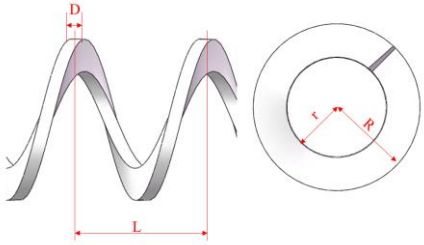

a) Front view b) Side view

Fig. 2 - Schematic Diagram of Shaftless Screw Blade Structure

D - Thickness of screw blade; L - Pitch; R - Outer diameter of screw blade; r - Inner diameter of screw blade

The outer diameter D, inner diameter d, pitch L, and operating speed n of the shaftless screw conveyor should satisfy equations (1) to (4) respectively (*Xiang et al, 2010*; *Erhie et al, 2021*).

Screw outer diameter:

$$D \geq K\left[\frac{Q}{\varphi\rho C}\right]^{\frac{2}{5}} \tag{1}$$

In the equation, D represents the outer diameter of the screw blade in meters (m); K is the material characteristic coefficient, taken as 0.049; φ is the fill coefficient, taken as 0.3; ρ is the material unit bulk density, 407.9 kg/m^3; C is the inclination coefficient, taken as 1 when horizontal; Q is the screw conveying capacity, in this device, Q has been verified by the previous test, and its conveying capacity is 2.88 kg/h when it meets the process requirements of the device.

Screw inner diameter:

$$d = (0.2 \sim 0.35)\, D \tag{2}$$

Pitch:

$$L = (0.5 \sim 2.2)\, D \tag{3}$$

Operating speed:

$$n \leq \frac{\mathrm{A}}{\sqrt{D}} \tag{4}$$

In the equation, n represents the operating speed in revolutions per minute (r/min), A is the comprehensive material coefficient, taken as 50. The selection of K, φ, ρ, C, and A can be referenced from relevant literature (*Zhang et al, 2010; Bates, 2008*).

According to equation (1), the outer diameter of the shaftless screw blade only needs to be greater than 11 mm to meet the design requirements. The width of the material inlet of the vibrating feeder is 45 mm. To prevent material from blocking and overflowing on the chute, the maximum outer diameter of the shaftless screw blade is set to 30 mm. To avoid material flow obstruction inside the shaftless screw blade, based on the material's flow characteristics, the minimum flow space for the material should be at least 3 times the size of the material particles (*Zhu et al, 2023*).

Thus:

$$D \geq 3m \tag{5}$$

In the equation, m represents the average diameter of the material, in millimetres (mm).

The average diameter of the large particles of the ground material from the type I mill used in the experiment is 6.6 mm. Therefore, the minimum outer diameter of the selected screw blade is 19.8 mm.

Substituting the range of screw blade outer diameters, 19.8 to 30 mm, into equation (4), the operating speed should be 288.68 to 355.34 r/min. To ensure the strength and flexibility of the screw blade, a thickness of 2 mm (e) is selected for the screw blade. Based on practical usage, for equations (2) and (3), d is taken as $0.3D$ and L is taken as $0.5D$, which means the inner diameter of the screw blade ranges from 5.94 to 9 mm, and the pitch ranges from 9.9 to 15 mm. According to Ji, the gap between the screw outer diameter and the barrel wall has a significant impact on the conveying efficiency and operating power (*Ji, 2021*). When designing screw conveyors, the gap should be smaller than the size of the particles to reduce power consumption and material damage. Considering this, a gap of 2 mm between the screw outer diameter and the barrel wall is selected.

Simulation Experiment

To explore the optimal operating conditions of the shaftless screw blades, simulation experiments are conducted on the screw pitch, outer diameter of the screw blades, inner diameter of the screw blades, and blade rotation speed. The aim is to determine the optimal combination of parameters for the screw blades.

Simulation Model

This design focuses on the sub-material of the Type I skin mill. The "Polyhedral" particle model, newly added in EDEM 2022, is adopted. Figure 3(a) shows the plan view and front view of the particles under the Type I skin mill, presenting an overall "rectangular prism" shape. After measuring the length, width, and height of 100 sub-material particles, their average dimensions are determined to be 6.3 mm, 3.7 mm, and 1.2 mm, respectively. Ultimately, the simulated particle model adopts the particles shown in Figure 3(b), with their dimensions set to the measured average values. Referring to the contact parameter determination method in the GEEM library and literature (*Li et al, 2019; Chen et al, 2023; Hoshishima et al, 2021*), the contact parameters between the sub-material particles and stainless steel are measured, as shown in Table 1. The calibration method of discrete element parameters for sub-material particles and experimental details will be reported separately.

a) Physical particles *b) Simulated particle*

Fig. 3 - Ground down actual and simulated particles

Table 1

EDEM simulation model parameter

Item	Argument	Numerical value
Ground stock	**Poisson's ratio**	0.33
	Shear modulus /[Pa]	2.088×10^{8}
	density /[kg/m^3]	1270
Stainless steel	**Poisson's ratio**	0.274
	Shear modulus /[Pa]	7×10^{10}
	density /[kg/m^3]	7800
Ground stock - Ground stock	**Collision recovery coefficient**	0.241
	Static friction factor	0.619
	Rolling friction factor	0.055
Ground stock - Stainless steel	**Collision recovery coefficient**	0.176
	Static friction factor	1.364
	Rolling friction factor	0.399

The simplified simulation model of the sampling component built in SolidWorks is imported into EDEM, as shown in Figure 4. To ensure the accuracy of the experiment, material particles are generated with a normal distribution. The particle factory is set above the inlet, and a flow detection sensor is added at the end of the shaftless screw sampler for convenient processing of the experimental results. The sensor captures the conveying capacity for 8 seconds and calculates the average value. Simulation parameters are set according to the experimental plan, with a total simulation duration of 15 seconds.

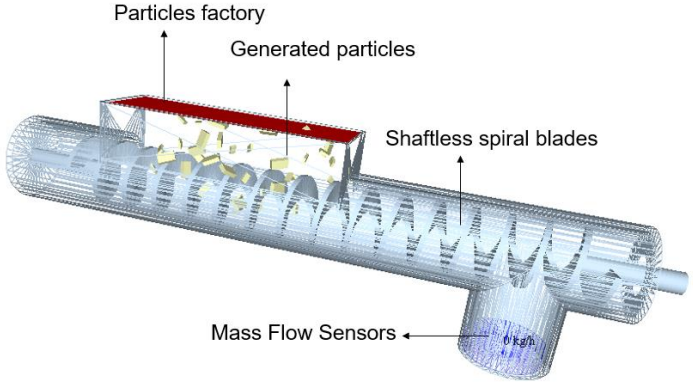

Fig. 4 - Simulation Model of Shaftless Screw

Experimental Factors and Experimental Indicators

As deduced from the parameter design in the previous section, the conveying capacity of the shaftless screw blade is related to the outer diameter, inner diameter, pitch, and rotational speed of the screw blade. To find the optimal parameters for the shaftless screw blade, Design Expert 13 is used to analyse these four influencing factors through experimental trials. The ranges of the outer diameter, inner diameter, pitch, and rotational speed of the screw blade are set to 19.8-30 mm, 5.94-9 mm, 9.9-15 mm, and 288.68-355.34 r/min respectively.

RESULTS

Box-Behnken Combination Experiment

Based on the designed ranges of four influencing factors mentioned earlier, Design Expert 13 was employed to conduct a Box-Behnken experiment with four factors at three levels. The independent variables included the outer diameter of the helical blade, the inner diameter of the helical blade, the pitch, and the rotational speed of the helical blade. The response value was the conveying capacity at the end of the shaftless spiral feeder. The aim was to seek the optimal operating parameters for the shaftless helical blade. The experiment consisted of 29 simulation runs, with 5 sets of trials established at the central level. The experimental factors and their codes are shown in Table 2, and the experimental results are presented in Table 3.

Table 2

Experimental Factors and Codes

Code	Factor			
	Spiral blade outer diameter *A* / [mm]	**Spiral blade inner diameter *B* / [mm]**	**Pitch of spiral *C* / [mm]**	**Rotational speed of spiral blades *D* / [r·min^{-1}]**
1	30	9	15	355.34
0	24.9	7.47	12.45	322.01
-1	19.8	5.94	9.9	288.68

Table 3

Experimental Results and Design

Serial number	Spiral blade outer diameter *A*	Spiral blade inner diameter *B*	Pitch of spiral *C*	Rotational speed of spiral blades *D*	conveying capacity *Y*/[kg/h]
1	24.9	7.47	12.45	322.01	9.527
2	30	7.47	15	322.01	11.761
3	30	7.47	12.45	288.68	10.527
4	24.9	7.47	15	288.68	7.217
5	24.9	5.94	12.45	355.34	6.731
6	24.9	9	12.45	355.34	4.663
7	24.9	5.94	15	322.01	8.639
8	30	7.47	12.45	355.34	12.638
9	24.9	7.47	12.45	322.01	8.006
10	19.8	7.47	12.45	288.68	3.58
11	24.9	7.47	12.45	322.01	9.987
12	24.9	5.94	9.9	322.01	4.378
13	24.9	7.47	12.45	322.01	8.033
14	19.8	7.47	9.9	322.01	2.226
15	19.8	7.47	12.45	355.34	7.233
16	24.9	7.47	15	355.34	10.967
17	24.9	7.47	12.45	322.01	7.842
18	24.9	9	15	322.01	11.53
19	24.9	7.47	9.9	355.34	10.059
20	30	7.47	9.9	322.01	6.213
21	19.8	7.47	15	322.01	9.589
22	24.9	7.47	9.9	288.68	2.131
23	24.9	5.94	12.45	288.68	3.628
24	24.9	9	12.45	288.68	2.484
25	19.8	9	12.45	322.01	6.377
26	24.9	9	9.9	322.01	3.435
27	19.8	5.94	12.45	322.01	10.777
28	30	9	12.45	322.01	9.661
29	30	5.94	12.45	322.01	10.231

Using Design Expert 13 to analyse the experimental results, the analysis of variance is shown in Table 4. Additionally, the response surface regression equation for the conveying capacity, given by equation (6), is obtained.

Table 4

Analysis of Variance

Source	Sun of Squares	df	Mean Square	*F*	*P*
Model	214.77	14	15.34	3.40	0.0144
A	37.63	1	37.63	8.34	0.0119
B	3.24	1	3.24	0.7180	0.4110
C	81.44	1	81.44	18.06	0.0008
D	43.03	1	43.03	9.54	0.0080
AB	3.67	1	3.67	0.8130	0.3825
AC	0.8236	1	0.8236	0.1826	0.6757
AD	0.5944	1	0.5944	0.1318	0.7220
BC	3.67	1	3.67	0.8147	0.3820
BD	0.2134	1	0.2134	0.0473	0.8309
CD	4.36	1	4.36	0.9675	0.3420
A²	5.26	1	5.26	1.17	0.2984
B²	12.43	1	12.43	2.76	0.1191
C²	3.02	1	3.02	0.6705	0.4266
D²	13.99	1	13.99	3.10	0.1000
Residual	63.15	14	4.51		
Lack of Fit	59.15	10	5.91	5.91	0.0507
Pure Error	4.00	4	1.00		
Cor Total	277.92	28			

$$Y=8.68+1.77A-0.5195B+2.61C+1.89D+0.9575AB-0.4537AC-0.3855AD+0.9585BC-0.2310BD \quad (5)$$
$$-1.04CD+0.9007A^2-1.38B^2-0.6828C^2-1.47D^2$$

In the equation, A, B, C and D are coded values.

Response Surface Analysis

Using Design Expert, response surface plots are obtained to illustrate the effects of various interaction factors on the conveying capacity, as shown in Figure 5. In the plot, factors other than the interaction factors are kept at their midpoint values.

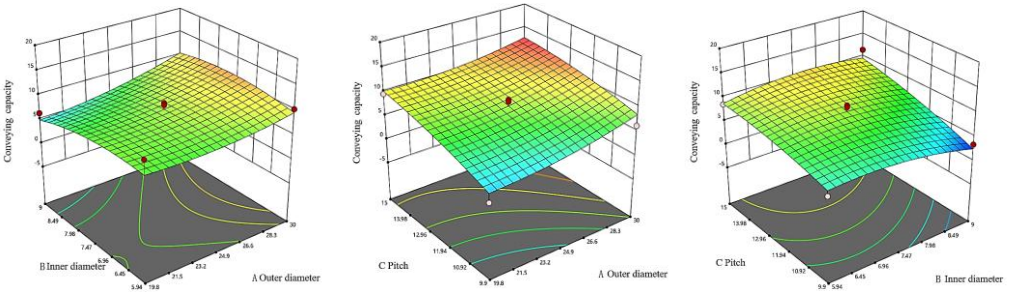

a) AB **b) AC** **c) BC**

Fig. 5 - The effects of the AB, AC, and BC interactions on the conveying capacity

As shown in Figure 5(a), the conveying capacity of the screw device increases steadily with the increase in blade outer diameter. Analysing the reason, with the increase in blade outer diameter, the filling volume of the material inside the screw device increases, thereby improving the conveying capacity of the screw mechanism. When the blade outer diameter is small, the conveying capacity of the screw mechanism decreases with the increase in blade inner diameter, and the rate of decrease becomes faster after reaching a certain value. Analysing the reason, with the increase in blade inner diameter, the gap inside the mechanism increases, resulting in increased fluidity of the material inside the screw device, thereby reducing the conveying capacity. When the blade outer diameter is large, the conveying capacity increases with the increase in blade inner diameter, but after reaching the peak, it slowly decreases. Analysing the reason, when the outer diameter is large, with the increase in inner diameter, the filling volume of the material inside the screw increases. However, after exceeding a certain degree, the increase in fluidity of the material has a more significant impact on the conveying capacity.

As shown in Figure 5(b), the curvature of the contour lines for the AC interaction is lower compared to those for the AB and BC interactions, indicating that the interaction between AC is not as significant as the other two groups. The conveying capacity of the screw device increases steadily with the increase in blade outer diameter. The conveying capacity of the screw device increases with the increase in pitch. Analysing the reason, with the increase in pitch, the gaps for material filling gradually increase, and more material fills the spaces between the screws, thereby increasing the conveying capacity of the material. This is similar to the findings in Figure 5(a).

As shown in Figure 5(c), the conveying capacity of the screw device gradually decreases with the increase in inner diameter and increases with the increase in pitch. This is similar to the findings in Figure 5(a).

Targeting the optimization of the objective function, using the Optimization function in Design Expert 13 with a target conveying capacity of 2.88 kg/h, the optimal combination parameters obtained are as follows: A (blade outer diameter) = 23.8 mm, B (blade inner diameter) = 6.4 mm, C (pitch) = 11.2 mm, D (blade speed) = 288.9 r/min. Conducting experiments based on the optimal combination parameters yields a conveying capacity of 2.85 kg/h, with an error of 1.04% compared to the predicted value. The experimental and predicted values are consistent, providing a reference for the design of the screw conveyor.

OPTIMIZED PARAMETER BENCH TRIAL

Experimental Material and Equipment

Using laboratory-made Type I skin mill sub-material that complies with production standards as the experimental material, as shown in Figure 6; applying a prototype of the self-made wheat milling sub-material particle size detection device for the throughput capacity test on the test stand, the experimental setup of the device feeding component test stand is depicted in Figure 7, with some structures made transparent for ease of experimental observation.

Experimental Design and Methodology

The experimental setup involves uniformly pouring the test material above the inlet. To accurately measure the feeding component's throughput over a unit of time and assess the overall operational stability of the device, the vibration feeder within the device is also activated and its conveying parameters are set. The material will then fall into the receiving bin at the end of the vibration feeder. To ensure precision in the experiment, timing starts the moment the material reaches the receiving bin. The experiment consists of 5 sets, with each set lasting 5 minutes.

The evaluation criterion used in this experiment is the coefficient of variation (CV) of throughput uniformity. A smaller coefficient of variation indicates less fluctuation in the feeding component's throughput, signifying more uniform feeding. The CV is calculated for each set of 5 statistical time periods, with each period lasting 15 seconds. During each time period, material is manually collected using a material receiving device. The calculation for the coefficient of variation is as follows:

$$\bar{m} = \frac{\sum_{i=1}^{x} m_i}{x} \quad i=1,2,...,5 \tag{6}$$

$$s = \sqrt{\frac{\sum_{i=1}^{x} (m_i - \bar{m})^2}{x-1}} \quad i = 1,2,...,5 \tag{7}$$

$$\delta = \frac{s}{\bar{m}} \times 100\% \tag{8}$$

In the equation,

$\bar{m}$ represents the average throughput within five-time intervals, g;

m_i represents the throughput within the i-th time interval, g;

x represents the quantity within the statistical time interval, where n equals 5;

s represents the standard deviation of throughput within each statistical time interval of a set of experiments, g;

δ represents the coefficient of variation of throughput uniformity, expressed as a percentage, %.

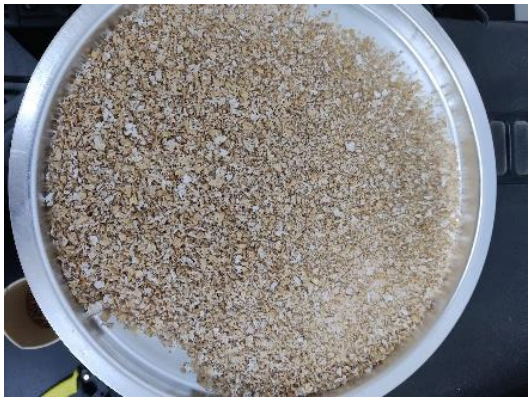

Fig. 6 - Laboratory-made material

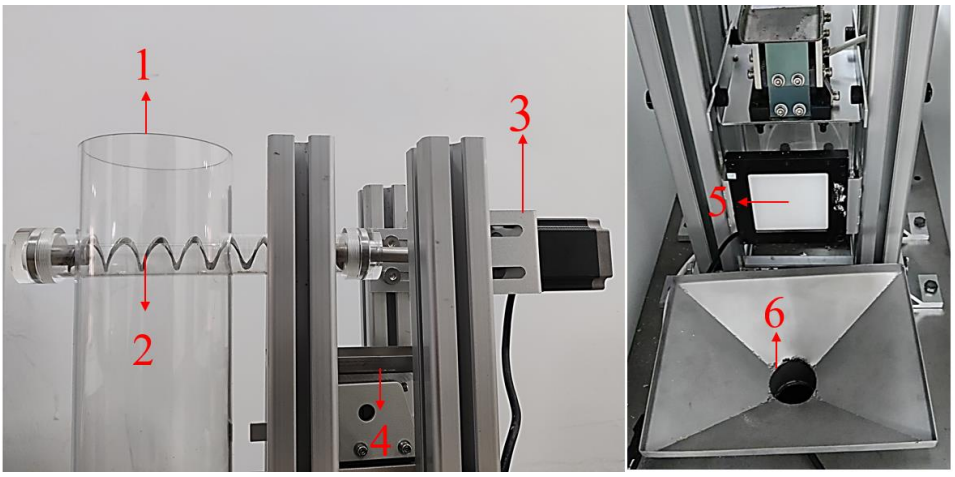

Fig. 7 - Bench Trial

1- Inlet; 2- Sampling Screw; 3- Drive Motor; 4- Vibrating Feeder and its Chute; 5- Backlight; 6- Receiving Hopper

Experimental Results and Analysis

The experimental results of the test stand are shown in Table 5.

Table 5

Bench trial data

Number of times	Conveying capacity / [kg/h]	Coefficient of variation of uniformity / %
1	2.71	1.34
2	2.83	1.28
3	2.81	1.42
4	2.91	1.29
5	2.79	1.33
Average value	2.81	1.33

According to Table 5, the average throughput capacity of the sampling device is 2.84 kg/h, the coefficient of variation of uniformity for the five experiments is 1.33%, indicating good stability in the operation of the device. The discrepancy may be attributed to measurement errors or insufficient material dispersion during manual operation, which affected its throughput performance. However, it still meets the requirements for device usage.

The results from both the Box-Behnken combination experiment and the parameter optimization bench test indicate that the designed parameters, with a helical blade outer diameter of 23.8 mm, inner diameter of 6.4 mm, pitch of 11.2 mm, and blade speed of 288.9 r/min, can be effectively implemented in the design of this apparatus. They satisfactorily meet the design requirements for the feeding components of the device. Additionally, this chapter conducts an analysis of the response surface experiment results, providing some guidance for the design optimization of the shaftless helix. Furthermore, the similarity between the research outcomes of this study and those documented in relevant literature (*Ma et al, 2019; Zhu et al, 2023; Wulantuya et al, 2020*) validates the correctness of the research content and results presented in this paper.

CONCLUSIONS

This study focuses on the shaftless screw blades of the spiral feeding component in the wheat processing particle size online detection device, with the throughput capacity of the screw conveyor as the target. A Box-Behnken experiment with four factors and three levels is conducted using Design Expert 13. A quadratic regression equation is established, with a throughput capacity target of 2.88 kg/h.

The optimal parameter combination is determined to be: outer diameter of screw blades 23.8 mm, inner diameter of screw blades 6.4 mm, pitch 11.2 mm, and blade rotation speed 288.9 r/min. Simulation experiments based on the optimal parameter combination yield a throughput capacity of 2.85 kg/h for the screw blades, with a prediction error of 1.04%, validating the reliability of the multi-objective optimization model. Further experiments on the test stand using the optimal parameter combination show an average throughput capacity of 2.84 kg/h for the test stand prototype, with an average coefficient of variation of throughput uniformity in the test stand experiments of 1.33%, confirming the reliability of the device operation. Additionally, the assembly of the wheat processing particle size online detection device is completed, and the device operates smoothly with stable operation of the feeding components and no occurrence of material blockages.

ACKNOWLEDGEMENT

This research was supported by Training plan of young backbone teachers in colleges and universities in Henan Province (2020GGJS088), Opening subject of Henan key laboratory of grain and oil storage construction and safety (2021KF-B02), Science and Technology Research Project of Henan (No.232103810084) and Science and Technology Key Research Program of Henan Provincial Department of Education (24A460004)

REFERENCES

[1] Ananth V.L., Arun K.K., Shrivathsan S., et al. (2023). Design of shaftless spiral conveyor for transportation of bulk materials[C]//*AIP Conference Proceedings. AIP Publishing*, 2869(1).

[2] Bates L. (2008). Screw conveyors[J]. *Bulk solids handling: equipment selection and operation*: 197-220.

[3] Bangura K., Gong H., Deng R.L., et al. (2020). Simulation analysis of fertilizer discharge process using the Discrete Element Method (DEM) [J]. *PLoS One*, 15(7): e0235872.

[4] Bidas M, Galecki G. (2021). The concept of a screw conveyor for the vertical transport of bulk materials [J]. *Mining Machines*.

[5] Cheng Luyang, Zhao Chunhui, Wang Ke. (2016). Shaftless Screw Conveyor（无轴螺旋输送机） [J]. *Hoisting and Transporting Machinery,* (08):16-18.

[6] Chen Yong, Gao Xiaoxun, Jin Xin, et al. (2023). Parameter calibration and experiment of discrete element Simulation for the seeds of Yousa bean(油莎豆排种离散元仿真参数标定与试验)[J]. *Transactions of the Chinese Society for Agricultural Machinery*, 54(12):58-69.

[7] Erhie E.O., Hillsden D., Sidhu A.S., et al. (2021). *Shaftless Screw Conveyor Design* [J].

[8] Hoshishima C., Ohsaki S., Nakamura H., et al. (2021). Parameter calibration of discrete element method modelling for cohesive and non-spherical particles of powder [J]. *Powder Technology*, 386: 199-208.

[9] Jiang Xiang, Cai Jianrong, Sun Li, et al. (2020). Structure Optimization Design of shaftless Spiral Heating Conveyor for Sterilization Machine （杀菌机的无轴螺旋加热输送器结构优化设计）[J]. *Packaging and Food Machinery*, 38(01):42-46.

[10] Ji Yu. (2021). Numerical Simulation of particle flow characteristics in screw conveyor based on CFD-DEM（基于 CFD-DEM 螺旋输送机内颗粒流动特性数值模拟研究） [D]. *Northeast Petroleum University*.

[11] Li Fengli, Tao Yanhui, Chen Jianghui. (2019). Discrete element parameter calibration of sunflower seeds based on accumulation test（基于堆积试验的食葵种子离散元参数标定)[J]. *Journal of Agricultural Mechanization Research*, 46(09):209-215.

[12] Li Wenbo, Hao Bing, Zhao Hu, et al. (2021). Research and application of ore particle size image online analysis system（矿石粒度图像在线分析系统的研究与应用）[J]. *Mining Machinery*, 49(04):47-50.

[13] Ma Chao, Liu Fei, Zeng Ting, et al. (2019). Development of an active filling device for simulative lunar soil with shaftless spiral（无轴螺旋式模拟月壤主动填充装置研制）[J]. *Journal of Deep Space Exploration*, 6(01):57-62.

[14] Motaln M., Lerher T. (2024). Innovative Approaches to Wear Reduction in Horizontal Powder Screw Conveyors: A Design of Experiments-Guided Numerical Study[J]. *Applied Sciences*, 14(7): 3064.

[15] Orefice L., Khinast J.G. (2017). DEM study of granular transport in partially filled horizontal screw conveyors[J]. *Powder Technol*, 305: 347-356.

[16] Wang Mingfeng, Xu Qiang, Jiang Enchen et al. (2017). Design and pilot test of feeders for axial spiral continuous pyrolysis of biomass（生物质无轴螺旋连续热解装置送料器设计及中试）[J]. *Transactions of the Chinese Society of Agricultural Engineering*, 33(04):83-88.

[17] Wang R., Zhang W., Shao L. (2018). Research of ore particle size detection based on image processing [C] // *Proceedings of 2017 Chinese Intelligent Systems Conference: Volume II.* Springer Singapore, 505-514.

[18] Wang Z., Li D., Zheng X., et al. (2021). A novel coal dust characteristic extraction to enable particle size analysis [J]. *IEEE Transactions on Instrumentation and Measurement*, 70: 1-12.

[19] Wen Suorang, Yang Lei. (2013). Application of on-line particle size detection in flour production（浅谈在线粒度检测在面粉生产过程中的应用）[J]. *Grain Processing*, 38(04):17-19.

[20] Xiang Dongzhi, Xu Yuwei. (2010). Design parameter selection of spiral conveyer（螺旋输送机设计参数的选择和确定）[J]. *Cement Technology*, (1): 29－33.

[21] Yang Lin (2018). Research on Dynamic Image Particle Size and Shape measurement System（动态图像颗粒粒度粒形测量系统研究）[D]. *Shandong University of Technology*.

[22] Zhang Chen, Guo Weicheng, Zhang Kai et al. (2010). Determination and Optimization of Design Parameters of Vertical Screw Conveyor（垂直螺旋输送机设计参数确定与优化）[J]. *Machinery Design & Manufacture*, (10):56-58.

[23] Zhao Xuejing (2009). Study on equivalent grain size and equivalent grain size curve in wheat milling（小麦制粉中当量粒度与当量粒度曲线研究）[J]. *Food Processing*, 34(02):16-18+58.

[24] Zhu H., Wu X., Bai L., et al. (2023). Design and experiment of a soybean shaftless spiral seed discharge and seed delivery device[J]. Scientific Reports, 13(1): 20751.

[25] Wulantuya, Wang H., Wang C., et al. (2020). Theoretical Analysis and experimental study on the process of conveying agricultural fiber materials by screw conveyors[J]. *Engenharia Agrícola*, 40(5): 589-594.